ELSEVIER Nuclear Instruments and Methods in Physics Research A 434 (1999) 244–253

NUCLEAR INSTRUMENTS & METHODS IN PHYSICS RESEARCH Section A

www.elsevier.nl/locate/nima

Local and global performance of double-gap resistive plate chambers operated in avalanche mode

M. Abbrescia[a], A. Colaleo[a], G. Iaselli[a], F. Loddo[a], M. Maggi[a], B. Marangelli[a], S. Natali[a], S. Nuzzo[a], G. Pugliese[a,*], A. Ranieri[a], F. Romano[a], S. Altieri[b], G. Belli[b], G. Bruno[b], G. Gianini[b], S.P. Ratti[b], L. Viola[b], P. Vitulo[b], S. Sergueev[c]

[a]Dipartimento Interateneo di Fisica and Sezione INFN, Universita di Bari, via Amendola 173, Bari I-70126, Italy

[b]Dipartimento di Fisica Nucleare e Teorica and Sezione INFN, Pavia, Italy

[c]Joint Institute for Nuclear Research, Dubna, Russia

Received 4 October 1998; received in revised form 26 April 1999; accepted 30 April 1999

Abstract

Two large double-gap resistive plate chambers, with 2 and 3 mm gap widths, were tested to study their response uniformity when operated in avalanche mode. The effects of mechanical tolerances and the presence of the spacers is thoroughly examined. Results on efficiency and time resolution are presented. We find that average performance and response uniformity over the whole chamber surface are fully adequate to the requirements of future collider experiments. © 1999 Elsevier Science B.V. All rights reserved.

1. Introduction

Resistive Plate Chambers (RPCs) are well-known gaseous detectors of ionizing particle. They are characterized by a large area coverage (order of the m^2), time resolution better than 2 ns and space resolution of the order of the cm. For physics they have been used in several experiments (NADIR, FENICE, E771, WA92, E831, MINI [1–6]) and have been implemented in the L3 endcaps [7] and in the return yoke of the magnet in BABAR [8].

Recently RPCs have been approved as dedicated detectors for the muon trigger system at the future Large Hadron Collider (LHC) experiments: ATLAS [9] and CMS [10].

In these experiments, RPCs will be operated in avalanche mode, while in the previous ones they were operated in streamer mode. In avalanche mode, the useful range of operation is defined as the voltage range where efficiency is $>90\%$ and streamer probability is $<10\%$. Local nonuniformities in the gap width can cause this range to change from one region to another of a single detector, resulting in narrowing the overall operation range.

Since the gap width is defined by a 10×10 cm^2 array of 1.2 cm diameter spacers, it is crucial to verify whether the technology used at present in the mass production meets the requirements of uniform response over areas of several square meters.

In this paper, a detailed study on efficiency and time properties of two double-gap chambers, as developed in the context of the CMS R&D project,

* Corresponding author. Tel.: + 39-80-544-3203; fax: + 39-80-544-2434.

E-mail address: gabriella.pugliese@ba.infn.it (G. Pugliese)

PII: S0168-9002(99)00534-3

is presented. Section 2 describes the experimental set-up and the methods used for this test; results on local and global efficiency are reported in Section 3; Section 4 presents the results on time properties.

Particular attention is given to the comparison of local and global performance of each chamber. A preliminary study has already been presented in [11]; progresses is discussed in Section 5.

2. Experimental set-up

The test described in this paper has been carried out on two double-gap 130×120 cm^2 chambers, the first equipped with 2 mm gap RPCs, the second with 3 mm gaps. The electrode plates were made of bakelite of nominal resistivity $\sim 2 \times 10^{11}$ Ω cm, without linseed oil surface treatment [12]. The sensitive volume was filled with a $C_2H_2F_4$/iso-C_4H_{10} 90%/10% gas mixture. Although this mixture is flammable and will not be used by CMS, it has been chosen to have backward compatibility with data collected in previous tests.

The spacers that define the gaps width were selected with a tolerance of ± 20 μm around the nominal value (2 or 3 mm) [13]. In the present design they had 12 mm diameter and were distributed on a 10×10 cm^2 grid so that they overlapped when the RPCs were superimposed to form the bi-gap.

Signals were read-out by means of 3.5×130 cm^2 aluminium strips, located between the two RPCs forming the chamber. They were terminated at one end on a 40 Ω resistor. At the other end, the strips were connected to a hybrid charge amplifier with 40 Ω input impedance, 10 MHz bandwidth, 1.5 ns rise-time of delta response and ~ 1.6 mV/fC sensitivity. Output signals were discriminated by a 30 mV threshold (corresponding to about 20 fC) and input to a multi-hit TDC (LeCroy 3377A), with a 512 ns time window and 0.5 ns sensitivity, operated in common stop mode. Each channel could register up to 16 hits before the trigger signal stopped the DAQ cycle.

The test has been carried out during the summer 1997, at the CMS-H2 beam line of the CERN SPS. A 220 GeV/c muon beam, characterized by a roughly Gaussian spatial profile with $\sigma \approx 2$ cm, was used. The beam intensity around the maximum was about 200 Hz/cm^2 (constant during all runs) and was measured by two 2×2 cm^2 scintillators located just downstream the RPCs. Another set of two 10×10 cm^2 scintillators gave the trigger, characterized by a jitter smaller than 0.5 ns. The beam spill was 2.5 s long.

To scan different regions, the chambers were displaced horizontally and vertically (X and Y axis). In total, 30 different 10×10 cm^2 regions were scanned, corresponding to about 20% of the whole sensitive area of the RPCs, as shown in Fig. 1.

2.1. Experimental methods

Two drift chambers [14] were used to determine the space (± 1 mm) coordinates of the muons crossing the RPCs and to predict the position of the fired strips.

The applied procedure of alignment consisted in minimizing, during the data analysis, the difference between the crossing points, extrapolated with the drift chambers, and the RPCs signal position on fired strips.

The chambers were considered efficient if the predicted strip, or the adjacent one closest to the reconstructed point, gave a signal detectable in a 60 ns window centered around the observed time distributions. The selected events were used to study also the time properties.

When more than one strip was fired, time properties were studied considering only the fastest signal. To compute the fraction of accidental coincidences biasing the evaluation of chambers performance, the same procedure was applied to events acquired with a random trigger. The percentage of accidentals was found to be less than 0.2%.

Each trigger area was then subdivided in 1×1 cm^2 squares to study local effects on efficiency and timing.

3. Efficiency

We first report the results obtained in the trigger region located in the middle of the chambers

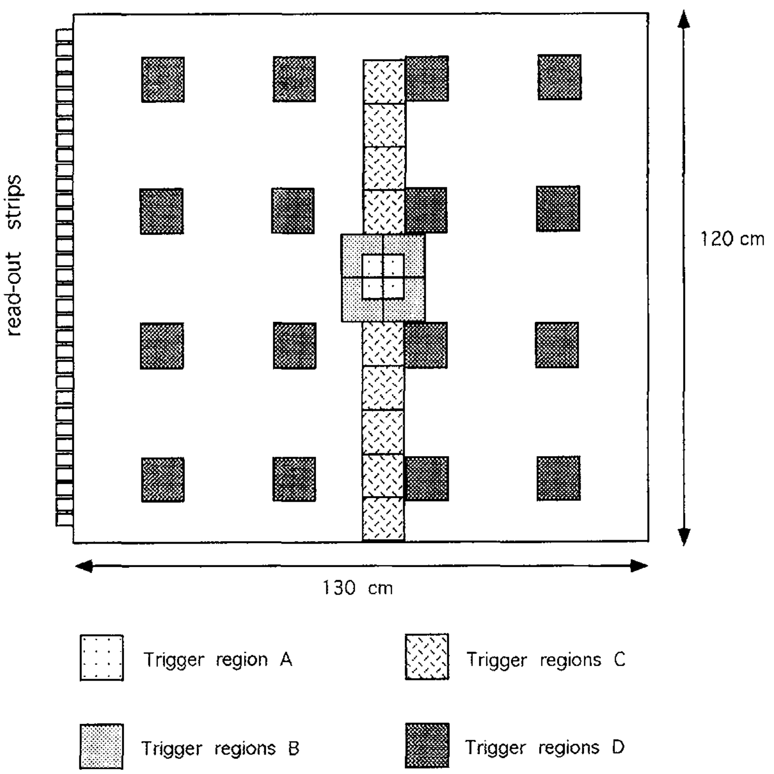

Fig. 1. Schematic view of the RPC with the trigger regions in evidence.

(region "A" in Fig. 1), having the spacers at the four corners. Global efficiency is evaluated as the average of local efficiencies over all the 1×1 cm^2 cells. This procedure simulates a uniform illumination on this 10×10 cm^2 region and ensures that the result is independent of the beam profile.

The response uniformity has been studied by computing cell-to-cell efficiency fluctuations around the average. An upper and a lower estimate of these fluctuations was obtained defining the following "up" and "down" variances:

$$\sigma^2_{\mathrm{up}} = \frac{1}{N}\sum_i^{\varepsilon_i > \bar{\varepsilon}} (\varepsilon_i - \bar{\varepsilon})^2 \quad (1)$$

$$\sigma^2_{\mathrm{dw}} = \frac{1}{N}\sum_i^{\varepsilon_i < \bar{\varepsilon}} (\varepsilon_i - \bar{\varepsilon})^2 \quad (2)$$

where $\bar{\varepsilon}$ is the average efficiency over the whole trigger region, ε_i is the ith cell efficiency and N is the total number of cells.

These definitions were chosen since, above the plateau knee, the ε_i distributions being strongly asymmetric around 100% efficiency.

Figs. 2a and b show efficiencies versus operating voltage (HV) for the 2 and the 3 mm chambers, respectively; dashed lines represent local fluctuations around the average, computed as explained above. The difference ΔI between the in-spill and off-spill current drawn by each chamber is also shown.

The 3 mm chamber reaches full efficiency at a lower electric field with respect to the 2 mm one; this is also predicted by simulation studies [15]. In fact, for a given total amplification ηg (where η is the first effective Townsend coefficient and g is the gap width) more charge is induced in a wider gap, leading to higher efficiency at given threshold.

The effect of the spacers has been studied considering four adjacent trigger regions (regions "B" in

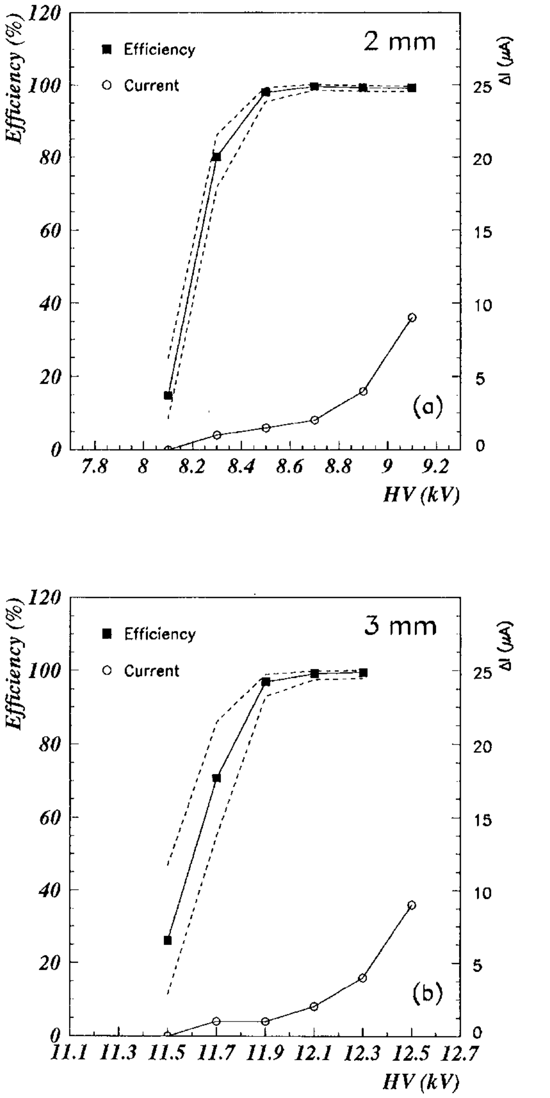

Fig. 2. Average efficiencies and currents versus HV for the 2 mm (a) and 3 mm (b) chambers in the central 10×10 cm^2 trigger region. Fluctuations around the average are shown.

Fig. 1, total area 20×20 cm^2) each centered on a spacer. The inefficiency map for the 2 mm chamber is shown in Fig. 3. In this figure, the area of each square is proportional to the inefficiency measured over the corresponding cells. The geometrical extension of the spacers accounts for the observed inefficiency. Similar results have been obtained for the 3 mm chamber.

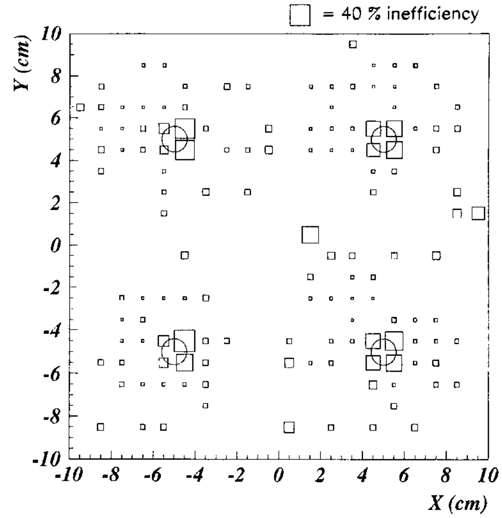

Fig. 3. Inefficiency map (2 mm, HV = 8.9 kV) in the central 20×20 cm^2 area of the chamber (circles represent the spacers).

To study the response uniformity on a whole chamber, several trigger regions were investigated. First, we considered nine regions located along a vertical line (Y direction, orthogonal to the strips) in the middle of the chambers (regions "C" in Fig. 1). Figs. 4 and 5 show the efficiency versus the position along the Y direction, at different HV, for the 2 and 3 mm chambers, respectively. The reported efficiencies are, again, the average values over the 100 basic cells into which each trigger region is subdivided. It can be clearly seen that, at increasing HV, point-to-point fluctuations tend to decrease becoming negligible at the detector working points.

Finally, all the regions labelled "D" in Fig. 1 were considered. The average efficiency over a total of 1600 cells is reported in Figs. 6a and b for the 2 and 3 mm chambers, respectively. Again, dashed lines indicate the fluctuations around the average, computed according to Eqs. (1) and (2).

The comparison between the curves reported in Figs. 2 and 6 shows that the fluctuations differ significantly; this means that long scale nonuniformities are also present and are by far more important than the short scale nonuniformities.

Although one might have expected the opposite effect, Figs. 2 and 6 show that, at low HV, the 3 mm

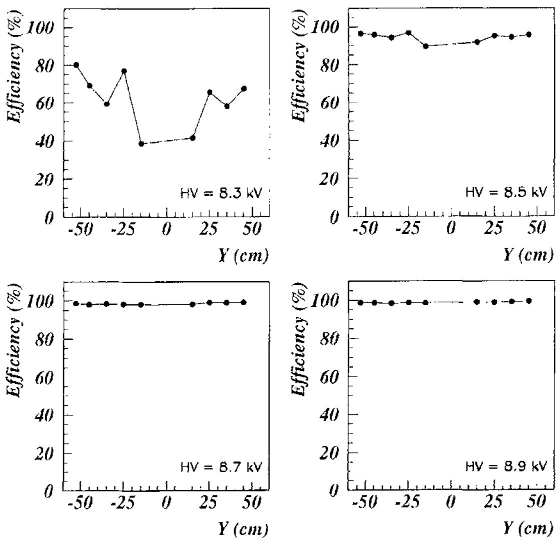

Fig. 4. Efficiency versus Y, at different HV for the 2 mm chamber. Each value is the average over 100 cells.

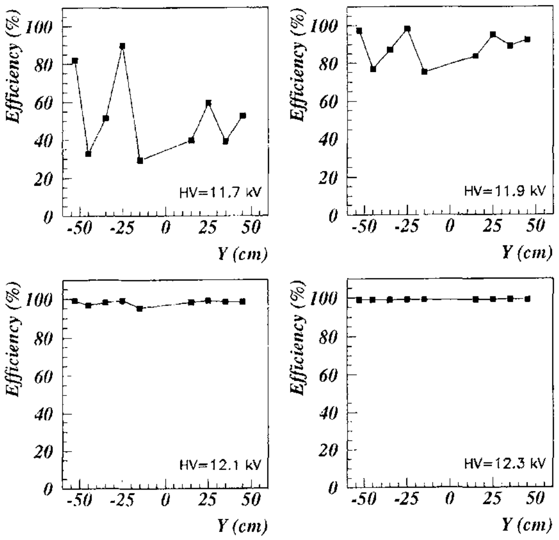

Fig. 5. Efficiency versus Y, at different HV for the 3 mm chamber. Each value is the average over 100 cells.

chamber efficiency has a slightly larger spread around the average. This could be due to the different treatment used in the construction of the 3 mm spacers, different from the one used for the 2 mm.

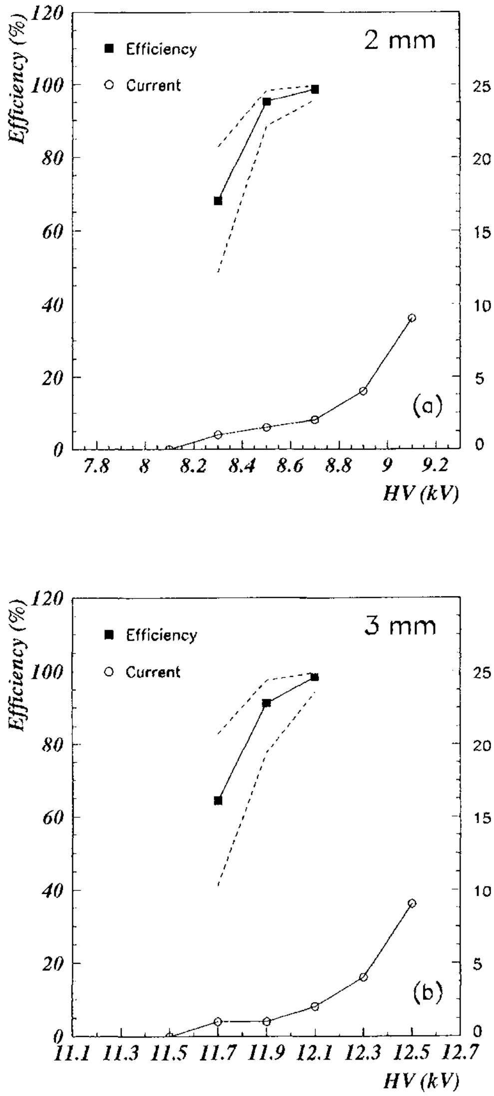

Fig. 6. Efficiencies versus HV for the 2 mm (a) and the 3 mm (b) chambers, computed as the average over 1600 cells.

4. Time properties

Good detector time properties are important for the performance of the muon trigger at future LHC experiments, where the short bunch crossing time separation (25 ns) imposes strict requirements on time resolution and "time walk". The time walk is defined as the variation of the signal average arrival time per unit of HV.

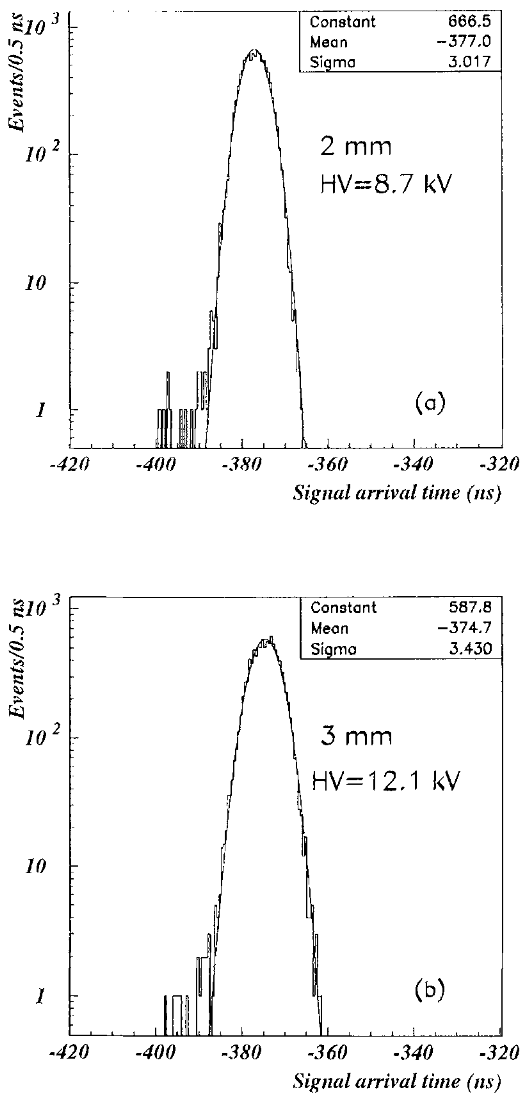

Fig. 7. Signal arrival time distributions (arbitrary zero) for the 2 mm (a) and the 3 mm (b) chambers.

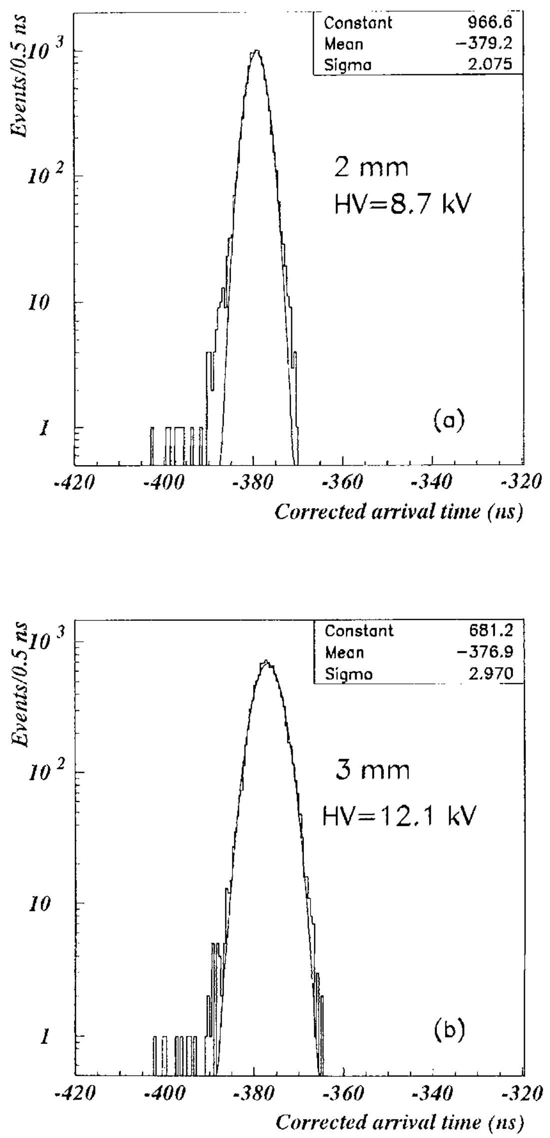

Fig. 8. Corrected signal arrival time distributions (arbitrary zero) for the 2 mm (a) and the 3 mm (b) chambers.

The time response has been studied extracting from the data an equal number of events for each of the 1600 (1×1 cm^2) cells belonging to the trigger regions "D". In this way the resulting hits are uniformly distributed over the investigated area.

The signal arrival time distributions (arbitrary zero) are shown in Figs. 7a and b for the 2 and 3 mm chambers, respectively. A Gaussian fit has been superimposed on each distribution. The sigmas of Gaussian fits are 3.0 (2 mm chamber) and 3.4 ns (3 mm chamber). As expected, the 3 mm one shows worse time resolution.

The tails on the left-hand side are consistent with the observed noise background and account for the cases in which the fastest hit in the 60 ns gate is not associated with a real track. Since only the fastest strip is considered for these distributions, a spurious hit can be observed on the right-hand side only if the chamber has not given a signal associated to

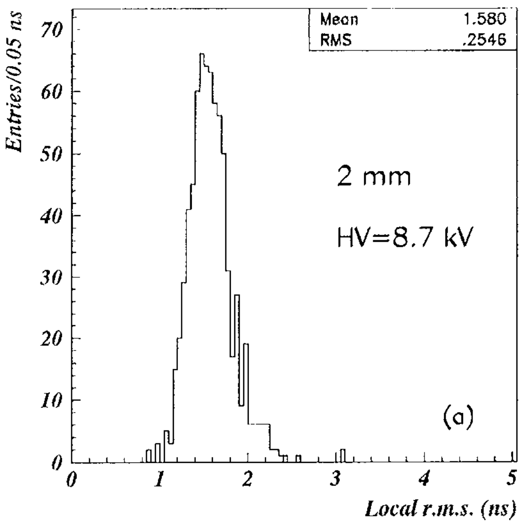

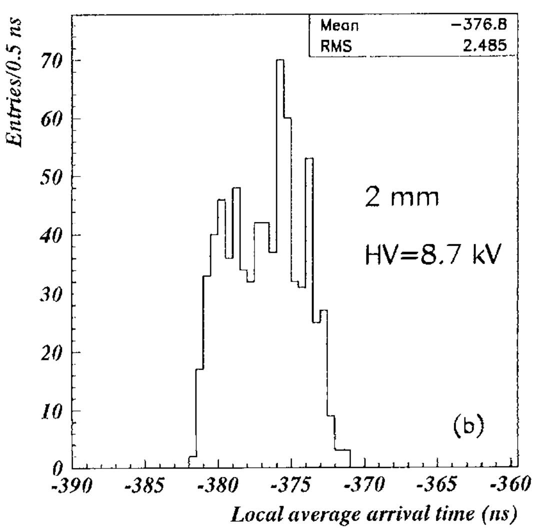

Fig. 9. Sigmas (a) and mean values (b) of the Gaussian fits to all the local (1×1 cm^2 cells) time distributions for the 2 mm chamber at HV = 8.7 kV.

the track; this is highly unlikely at the considered HV, since the chambers were almost fully efficient.

The overall time resolution is in general spoiled by both possible local nonuniformities and by the different signal propagation time along the read-out strips. The latter changes according to the avalanche location along the strip. Likewise, nonuniformities can cause the time response of the chamber to be different from one point to another. Both phenomena lead to a broadening of the overall time distribution.

The broadening effect due to the signal propagation time can be cancelled by subtracting the time needed by each signal to reach the front-end board. The corrected distributions, obtained assuming a signal speed along the read-out strips of 0.66 c, are shown in Figs. 8a and b for the 2 and 3 mm chambers, respectively. The value assumed for the signal propagation speed is consistent with the average shift of the signal arrival time observed in data samples taken at different positions along the read-out strips.

This procedure improves the time resolutions to 2.1 and 3.0 ns for the 2 and the 3 mm chambers, respectively.

As remarked previously, the time resolution would improve if local nonuniformities were absent. Time nonuniformities for the 2 mm chamber are shown in Figs. 9a and b. The corresponding plots for the 3 mm chamber are shown in Figs. 10a and b. In both chambers the spreads of sigma values are quite relevant and mean values distributions are wider than expected for perfectly uniform chambers.

The average value of the $\sigma_t^{(i)}$ distribution is 1.6 ns for the 2 mm and 2.0 ns for the 3 mm; these values can be referred to as the local time resolution of the detectors and are, of course, sensibly smaller than the global values reported above. The difference between local and global time resolution, after correction for the signal propagation time along the strips, is an indication of the degree of nonuniformity of the chambers.

In Figs. 11a and b results concerning the time resolution are summarized as a function of HV. The dashed lines above and below the local values select a ± 1 RMS area around the mean value. Time nonuniformities become smaller as HV increases.

In Figs. 12a and b the average arrival times are plotted as a function of HV for the 2 and 3 mm chambers. Both exhibit a time walk of approximately 13 ns/kV.

As already discussed in Section 3, the efficiency has been computed only considering signals in a suitably defined time window (gate). An inaccurate

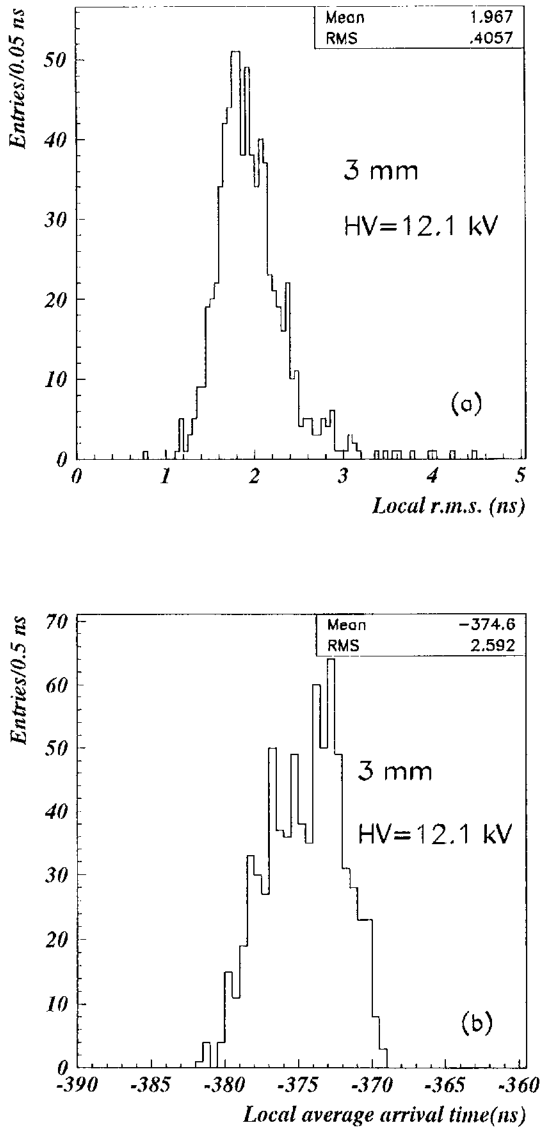

Fig. 10. Sigmas (a) and mean values (b) of the Gaussian fits to all the local (1×1 cm^2 cells) time distributions for the 3 mm chamber at HV = 12.1 kV.

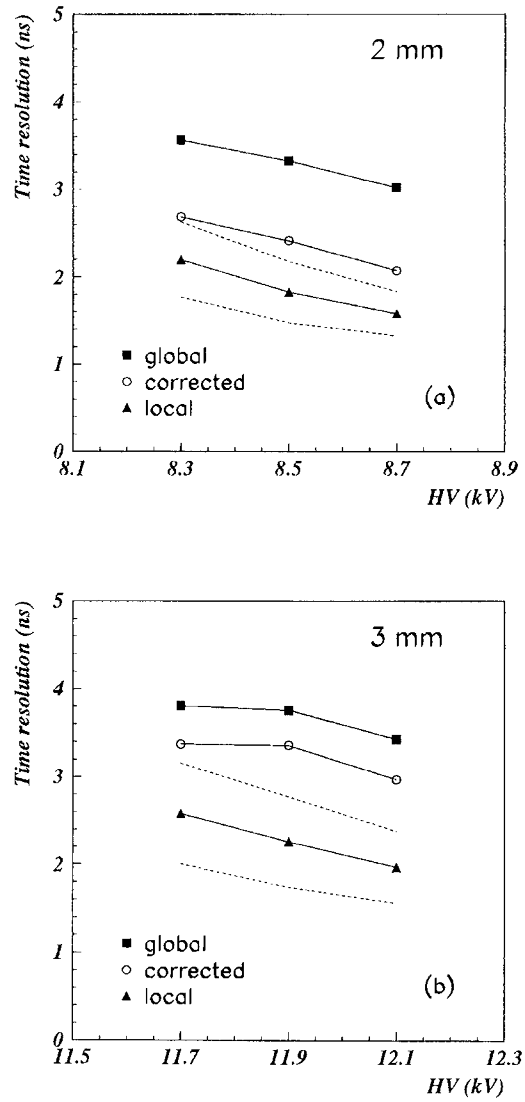

Fig. 11. Time resolution versus HV for the 2 mm (a) and the 3 mm (b) chambers.

positioning of the gate with respect to the signal arrival time may spoil achievable detector efficiency by rejecting out-of-gate signals. This is particularly important for operation at LHC, where only signals within a ~ 25 ns gate synchronized with the bunch crossing has been considered.

In Figs. 13a (2 mm) and b (3 mm), the chamber efficiency is plotted as a function of the time (arbitrary zero) at which a 25 ns gate is opened. To achieve efficiencies higher than 95%, the time plateau widths are limited to 15 (2 mm) and 13 ns (3 mm).

Recent simulation studies [16,17] concerning the RPC-based trigger system of CMS have indicated that, to provide an efficient trigger action, the

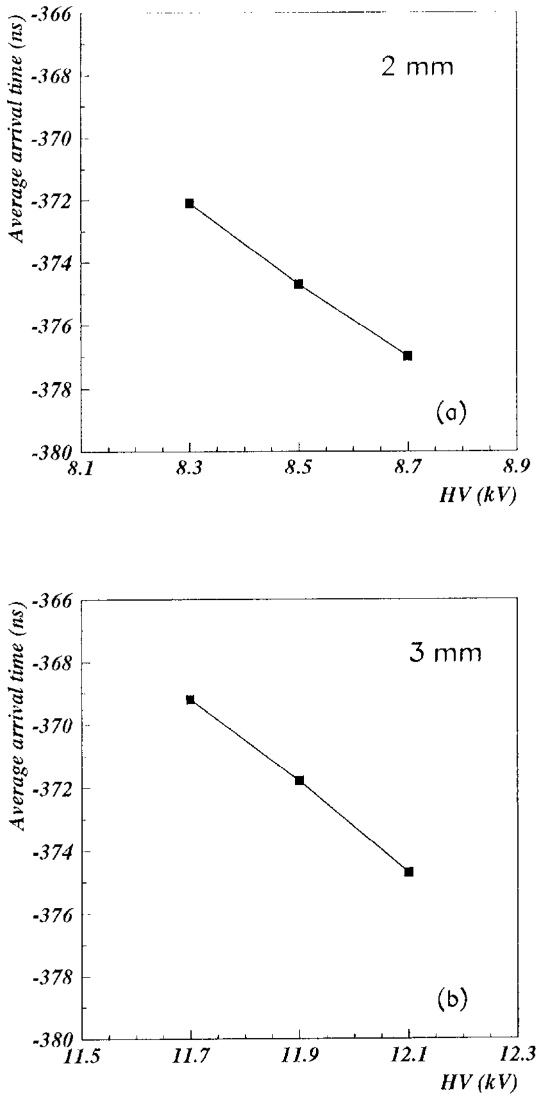

Fig. 12. Average arrival times (arbitrary zero) versus HV for the 2 mm (a) and the 3 mm (b) chambers.

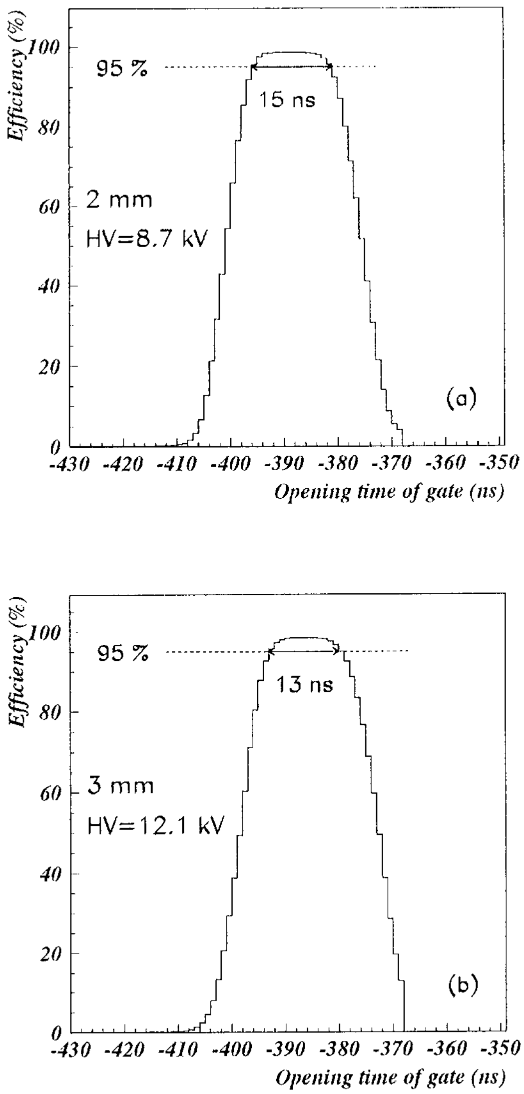

Fig. 13. Chamber efficiencies computed in a 25 ns gate as a function of the time at which the gate is opened.

chambers are required to have a time resolution, after subtracting signal propagation times, not exceeding 3 ns. Despite the existing nonuniformities, the tested 2 mm chamber ($\sigma_{corr} = 2.1$ ns at HV = 8.7 kV) has proven to fully satisfy these requirements. The 3 mm chamber is still within these limits, but exhibits worse time resolution ($\sigma_{corr} = 3.0$ ns at HV = 12.1 kV).

5. Conclusions

In this paper new results concerning double gap chambers operated in avalanche mode, as developed in the context of CMS R&D, have been presented.

Two chambers with RPC gap widths of 2 and 3 mm have been illuminated with a 200 Hz/cm^2 muon beam over a large fraction of their surfaces to study the response uniformity and to compare local and global performance.

Both chambers exhibit global properties adequate to the requirements of CMS: efficiency $> 98\%$ and time resolution < 3 ns. The main difference in their behaviour resides in the accuracy of their timing, which is better in the case of the 2 mm chamber (~ 2 ns) with respect to the 3 mm one (~ 3 ns).

We have found local variations (which however decrease with increasing HV), concerning both time resolution and efficiency. For example the time resolution, if computed in small cells, is considerably better than the quoted global values, and approaches the expected theoretical limits for this kind of detector [15].

This effect is certainly due to unavoidable variation of the gap thickness introduced both during the assembly of electrodes, and by the mechanical frame which supports the gaps which form the chamber. Therefore, care must be taken to limit the gap thickness tolerance to very small values and to make sure that mechanics does not introduce unnecessary strength which might locally deform the gaps.

To this respect, great progress has been made on the uniformity by releasing the "staggering" requirement of the spacers in the two gaps. Previous detectors were assembled in such a way that spacers in the two gaps did not overlap. This layout prevents the drop of efficiency to very low values in the regions where the spacers are located, since at least one gap is always sensible to the ionizing particle.

However, tests made on this double gap layout and extensively reported in a previous paper [12] have clearly shown that the uniformity response is very poor (compare Fig. 6 of the previous paper with Fig. 3 of the present paper). This is because, with no overlap, the strength of each spacer is transferred to the underneath gap, which is then deformed. Therefore the attempt to reduce the inefficiency to very low value by staggering the spacers was producing an overall degradation of the detector performance.

The new adopted geometry (with no staggering) has determined striking improvements in the uniformity of efficiency and time properties. The performance is presently well within the limits imposed for the construction of the large experiments at LHC.

Acknowledgements

We would like to thank G. Bencze for his continuous support during the measurements at the CMS-H2 beam line. We wish to acknowledge H. Fritz and his group for their assistance in data acquisition. We also thank the RPC Bari-Pavia technical staff for their important and efficient work.

References

[1] G. Bressi et al., Nucl. Instr. and Meth. A 261 (1987) 449.
[2] A. Antonelli et al., The FENICE detector at the e + e- collider ADONE, Nucl. Instr. and Meth. A 337 (1993) 34.
[3] E. Gorini, The Resistive Plate Counter muon system of E771, Nucl. Instr. and Meth. B (Proc. Suppl.) 23A (1991) 249.
[4] C. Bacci et al., Nucl. Instr. and Meth. A 324 (1993) 83.
[5] P.D. Sheldon, The FOCUS experiment RPC Muon identification array, in: S.P. Ratti, M. Merlo (Eds.), Proceedings of the III International Workshop on Resistive Plate Chambers and Related Detectors, 11–12 October 1995, Pavia, Italy, Scientifica Acta XI, 1996, pp. 437–444
[6] M. Abbrescia et al., Nucl. Instr. and Meth. A 336 (1993) 322.
[7] A. Aloisio et al., Nucl. Instr. and Meth. A 360 (1995) 340.
[8] The BABAR Collaboration, Technical Design Report, March 1995.
[9] ATLAS Technical Design Report, CERN/LHCC/97-22.
[10] CMS Technical Design Report, CERN/LHCC/97-32.
[11] M. Abbrescia et al., CMS Note 1997-062, Nucl. Instr. and Meth. A 414 (1998) 135.
[12] M. Abbrescia et al., Nucl. Instr. and Meth. A 394 (1997) 13.
[13] General Tecnica, Private Communication.
[14] A. Manarin, G. Vismara, The delay wire chamber description, LEP/BI-TA/Note 85-3.
[15] M. Abbrescia et al., Resistive Plate Chamber in avalanche mode: a comparison between model predictions and experimental results, Talk given at seventh Pisa Meeting on Advanced detectors, La Biodola, Isola d'Elba, Italy, 25–31 May, 1997, Nucl. Instr. and Meth. A 409 (1998) 1.
[16] G. Bruno et al., A simulation study of the RPC muon trigger for CMS, Proceedings of the IV International workshop on Resistive Plate Chambers and related detectors, 15–16 October 1997, Naples, Italy, Scientifica Acta, Vol. XIII, 1998, p. 377
[17] G. Bruno et al., CMS Internal Note 1998-004.